Human Molecular Genetics, 2012, Vol. 21, No. 10 **2219–2232**
doi:10.1093/hmg/dds037
Advance Access published on February 9, 2012

Marked differences in neurochemistry and aggregates despite similar behavioural and neuropathological features of Huntington disease in the full-length BACHD and YAC128 mice

Mahmoud A. Pouladi[1], Lisa M. Stanek[2], Yuanyun Xie[1], Sonia Franciosi[1], Amber L. Southwell[1], Yu Deng[1], Stefanie Butland[1], Weining Zhang[1], Seng H. Cheng[2], Lamya S. Shihabuddin[2] and Michael R. Hayden[1,*]

[1]Centre for Molecular Medicine and Therapeutics, University of British Columbia, and Child and Family Research Institute, Vancouver, BC, Canada and [2]Genzyme Corporation, Framingham, Massachusetts, USA

Received November 21, 2011; Revised January 13, 2012; Accepted February 6, 2012

The development of animal models of Huntington disease (HD) has enabled studies that help define the molecular aberrations underlying the disease. The BACHD and YAC128 transgenic mouse models of HD harbor a full-length mutant huntingtin (*mHTT*) and recapitulate many of the behavioural and neuropathological features of the human condition. Here, we demonstrate that while BACHD and YAC128 animals exhibit similar deficits in motor learning and coordination, depressive-like symptoms, striatal volume loss and forebrain weight loss, they show obvious differences in key features characteristic of HD. While YAC128 mice exhibit significant and widespread accumulation of mHTT striatal aggregates, these mHTT aggregates are absent in BACHD mice. Furthermore, the levels of several striatally enriched mRNA for genes, such as DARPP-32, enkephalin, dopamine receptors D1 and D2 and cannabinoid receptor 1, are significantly decreased in YAC128 but not BACHD mice. These findings may reflect sequence differences in the human *mHTT* transgenes harboured by the BACHD and YAC128 mice, including both single nucleotide polymorphisms as well as differences in the nature of CAA interruptions of the CAG tract. Our findings highlight a similar profile of HD-like behavioural and neuropathological deficits and illuminate differences that inform the use of distinct endpoints in trials of therapeutic agents in the YAC128 and BACHD mice.

INTRODUCTION

The development of a therapeutic compound from preclinical research into human clinical trials typically requires successful demonstration of therapeutic benefit in animal models of the disease. The discovery of the mutation in the Huntington disease (*HD*) gene in 1993 (1) resulted in the establishment of numerous animal models with a CAG expansion analogous to the human disease. Although genetic models of HD have been generated in lower invertebrates such as fruit flies and nematodes, transgenic mice expressing the mutant *HTT* gene, or a portion thereof, have been the most commonly used models to investigate potential therapies for HD.

In an effort to unravel mechanisms leading to disease, the ideal animal model of HD is likely to necessitate reproduction of the mutation in the context of the complete human gene. Various pathways dependent on sequences outside of the mutation itself might be appropriately regulated in this animal model, including post-translational modifications of HTT dependent on sequence in the human gene. In addition, the full-length human *HTT* gene along with sufficient upstream and downstream regulatory sequences would ensure appropriate cellular and temporal expression of the gene (2). The current mouse models show varying degrees of similarity to the human condition and each model has its advantages and disadvantages. Transgenic mice expressing mutant huntingtin

*To whom correspondence should be addressed at: Centre for Molecular Medicine and Therapeutics, University of British Columbia, 950 West 28th Avenue, Vancouver, BC, Canada V5Z 4H4. Tel: +1 6048753535; Fax: +1 6048753819; Email: mrh@cmmt.ubc.ca

(*mHTT*) N-terminal fragments, such as the R6/2 model, exhibit a number of HD-like phenotypes, including progressive motor deficits, striatal and cortical atrophy, shortened lifespan, reactive gliosis, mHTT aggregation and alterations in gene expression (3–5). Although these relatively acute and fast-progressing models have been used extensively for preclinical testing of drug candidates, they have limited predictive value for therapeutic success in patients with several compounds, such as ramecemide, coenzyme Q10 and riluzole, showing efficacy in these animal models but failing to confer benefits in clinical trials (6–10). Knock-in mouse models of HD have been established by replacing a portion of the mouse *Htt* gene with a portion of the mutant human copy that contains an expanded CAG region. These models, although harbouring the mutation seen in the human disease, demonstrate a very mild phenotype and protracted time course to disease onset, making them less convenient for efficacy testing *in vivo*. Other transgenic mouse models have been generated to express longer fragments or the full-length human mutant *HTT* gene. These include the yeast artificial chromosome (YAC) and bacterial artificial chromosome (BAC) mouse models (11–13), which contain the human mutation in the context of the complete human gene and show symptoms that closely parallel human HD such as progressive motor and cognitive abnormalities, psychiatric-like disturbances and striatal neuronal loss.

Both the YAC128 and BACHD mice express the entire human *HTT* gene containing 125 and 97 glutamine repeats, respectively, under the control of endogenous *HTT* regulatory machinery. These mice exhibit a predictable phenotype with age-dependent motor deficits, neuronal synaptic dysfunction and predominantly striatal atrophy and neurodegeneration. Characterization of the natural history of YAC128 and BACHD mice suggests that these are useful models for evaluation of therapeutic strategies for HD as they exhibit readily discernable and highly reproducible age-dependent disturbances in motor and cognitive function as well as selective neuronal atrophy. Despite these similarities, the YAC128 and BACHD mice are genetically distinct models. Methodologies for mouse model characterization have not been standardized and can vary greatly between laboratories. Here, we performed a direct comparison of the YAC128 and BACHD mouse models on the same background strain that were housed and tested under identical conditions in the same laboratory. We sought to evaluate the biochemical, behavioural and neuropathological profiles of both models and enrich our understanding of their similarities and differences in order to identify valuable endpoints that will allow for the efficient design and implementation of therapeutic trials in the YAC128 and BACHD mouse models.

RESULTS

Comparison of genomic sequence of the mHTT region in BACHD and YAC128 mice

As variations in gene sequence can influence the function of its protein product, we examined whether there are sequence differences in the *mHTT* region and its genomic context embedded in the BACHD and YAC128 mice that may contribute to phenotypic differences between these lines. The genomic insert containing the human *mHTT* gene in BACHD mice is ~240 kb in size compared with 308 kb in YAC128 mice (Table 1). This difference in genomic insert size reflects the inclusion of a larger genomic region upstream of the *mHTT* gene in YAC128 (24 kb) compared with BACHD mice (20 kb), as well as a larger genomic region downstream of the *HTT* gene in YAC128 (116.8 kb) compared with BACHD mice (50 kb) (Table 1). Single nucleotide polymorphisms (SNPs) spanning the entire *mHTT* region in both BACHD and YAC128 mice were genotyped (14). Of the 85 SNPs genotyped in both the YAC128 and BACHD transgenes, the alleles of 36 SNPs were found to differ between them. These included three missense amino acid differences, one allelic difference just upstream of the *HTT* 5′-UTR and one in the 3′ untranslated region (Fig. 1).

Table 1. Comparison of genomic features of constructs used to generate the BACHD and YAC128 mice

	BACHD	YAC128 (line 53)
Original construct		
Clone	BAC RP11-866L6	YAC 353G6
Insert size	~240 kb	308 kb
Length upstream of *HTT* gene	~20 kb	24 kb
Length downstream of *HTT* gene	~50 kb	116.8 kb
Transgene		
CAG repeats	97	125
Chromosomal localization	Not determined	3qB
*Lox*P sites	2 flanking exon 1	No
Copy number	~5	~4
Lines phenotypically analysed	2 (BACHD and BACHD-L)	3
SNPs		
Total SNPs compared	85	85
Total SNPs different	36	36
Promoter	1	1
Exonic	7 (1 in 3′ UTR)	7 (1 in 3′ UTR)
Intronic	23	23
Downstream (3′) sequences	5	5

Amino acid sequence differences

Using PolyPhen, a tool which uses physical and comparative considerations to predict the potential impact of an amino acid substitution on protein structure and function (15), two of the three identified missense differences were predicted to be benign: Tyr-His at rs362331 in exon-50 and Val-Ile at rs362272 in exon-61. One amino acid difference, however, is predicted to affect huntingtin protein function. At this SNP, rs34315806, which is located in exon 29 at amino acid 1262 of the HTT protein, BACHD harbours the G allele coding for Thr, which occurs in this position in the human and mouse reference sequences. The *mHTT* transgene in YAC128 has an A allele at rs34315806 coding for Met. This allele has a minor allele frequency of 0.067 in the Yoruban African population but is not observed in Caucasian European, Chinese or Japanese HapMap populations in dbSNP release 132 (16,17). We predict that this sequence difference, because it occurs in close proximity to HEAT-repeat region 3 (18), could conceivably influence HTT protein function by

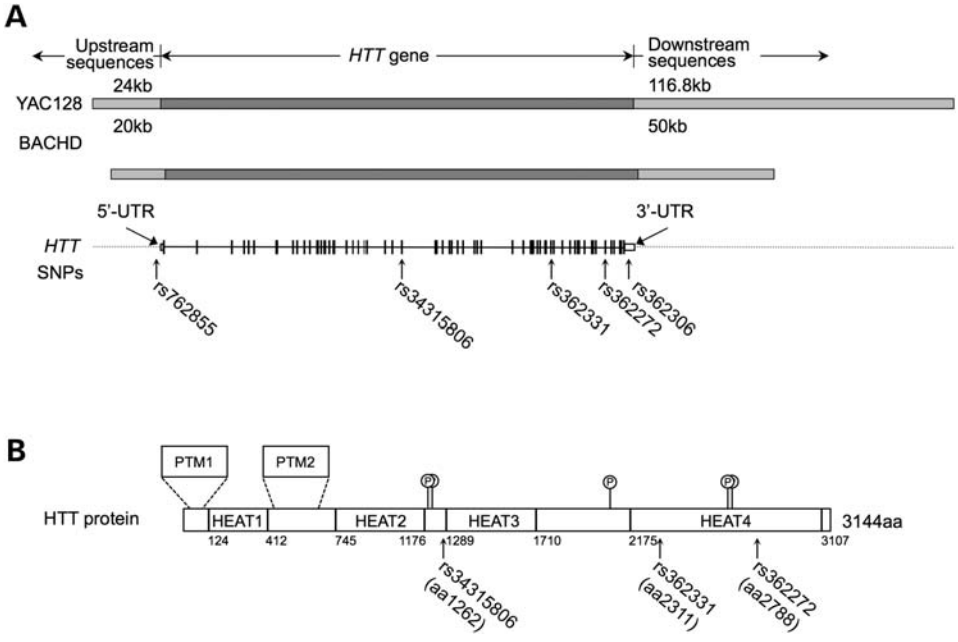

Figure 1. Comparison of genomic context of the *HTT* gene in BACHD and YAC128 mice and relationship of SNPs to HTT protein features. (**A**) The YAC128 and BACHD transgenes both contain the complete HTT gene, while YAC128 includes an additional 4 kb upstream and ~67 kb downstream of HTT. HTT coding exons are represented by vertical bars and 5′-UTR and 3′-UTR by open rectangles. Allelic differences at five SNPs could contribute to phenotypic differences between the YAC128 and BACHD mouse models: rs762855 is 1.6 kb upstream of the HTT transcription start site; rs34315806, rs362331 and rs362272 are coding SNPs; rs362306 is in the 3′-untranslated region of HTT. (**B**) SNPs that result in missense coding differences between BACHD and YAC128 are shown in the context of HTT protein features. PTM1 and PTM2 represent two major clusters of post-translational modifications including phosphorylation, ubiquitination, sumoylation and acetylation sites and protease cleavage sites (reviewed in 18). Individual phosphorylation sites further downstream are marked with 'P' in open circles. Amino acid (aa) locations of HEAT repeats 1 through 4 are marked below HTT.

influencing its binding with interactors. Consequently, it may contribute to phenotypic differences between BACHD and YAC128 mice, although additional studies would be needed to investigate this possibility. None of the three missense-coding differences between BACHD and YAC128 is close to the two major clusters of post-translational modifications in the HTT protein (Fig. 1B).

Putative regulatory differences

One SNP allele difference between the YAC128 and BACHD *mHTT* transgenes at rs762855 (~1.6 kb upstream of the *HTT* transcription start site) lies in a putative *HTT* regulatory sequence (19). Regulatory analysis of variation in enhancers (20) indicated that this SNP occurs in a conserved non-coding sequence and the alleles present in YAC128 and BACHD are predicted to differentially bind to the transcription factors Dorsal-1, Hen-1, Myf, Snail and Tal1beta-E47S. None of these has yet been specifically linked to *HTT* regulation or HD, but it is possible that this difference can result in spatial or temporal changes in *HTT* gene expression by influencing binding of specific transcription factors. Finally, SNP rs362306, which is different between YAC128 and BACHD, is located in the *HTT* 3′UTR, and does not overlap with any conserved miRNA-binding sites predicted by the TargetScan software for prediction of microRNA targets (21). As such, it is unlikely to contribute to any phenotypic differences between BACHD and YAC128 mice.

Comparison of the CAG tract sequence in the mHTT transgenes of BACHD and YAC128 mice

Genetic analyses of the human *mHTT* gene reveal that it contains a nearly pure tract of CAG that is interrupted by a penultimate CAA trinucleotide (22). To examine the similarities and differences in the composition of CAG/CAA within the CAG tracts in BACHD and YAC128 mice, the CAG tracts of the *mHTT* transgenes in both mice were sequenced.

The CAG tract of BACHD mice was determined to comprise 97 repeats containing 48 CAG repeats and 49 CAA repeats. A repeating sequence of 'CAG CAG CAA CAG CAA CAA' covers the entire stretch of the CAG tract with the exception of the first trinucleotide repeat which is represented by 'CAA' (Table 2). The CAG tract of YAC128 mice comprises 125 repeats containing 116 CAG repeats and 9 CAA repeats (Table 2). The nearly pure CAG tract in the *mHTT* transgene of the YAC128 is interrupted by two 'CAA CAA CAA CAG CAA' sequences at repeats 24–28 and 109–113, as well as a penultimate 'CAA' at repeat number 124 (Table 2). This configuration more closely resembles the CAG tract of the human *mHTT* gene.

Htt mRNA and protein levels in BACHD and YAC128 mice

To compare the level of Htt expression in BACHD and YAC128 mice, we employed real-time quantitative reverse transcription polymerase chain reaction (RT–PCR) and immunoblotting to measure mRNA and protein levels of

Table 2. Human *HTT* transgene CAG tract sequence in BACHD and YAC128 mice

	BACHD	YAC128
CAG tract length	97 repeats	125 repeats
Number of CAG trinucleotides	48	116
Number of CAA trinucleotides	49	9
Pattern	'CAG CAG CAA CAG CAA CAA' except at the following repeat number: 1: CAA	Pure CAG except at the following repeat numbers: 24–28: CAA CAACAA CAG CAA 109–113: CAA CAACAA CAG CAA 124: CAA

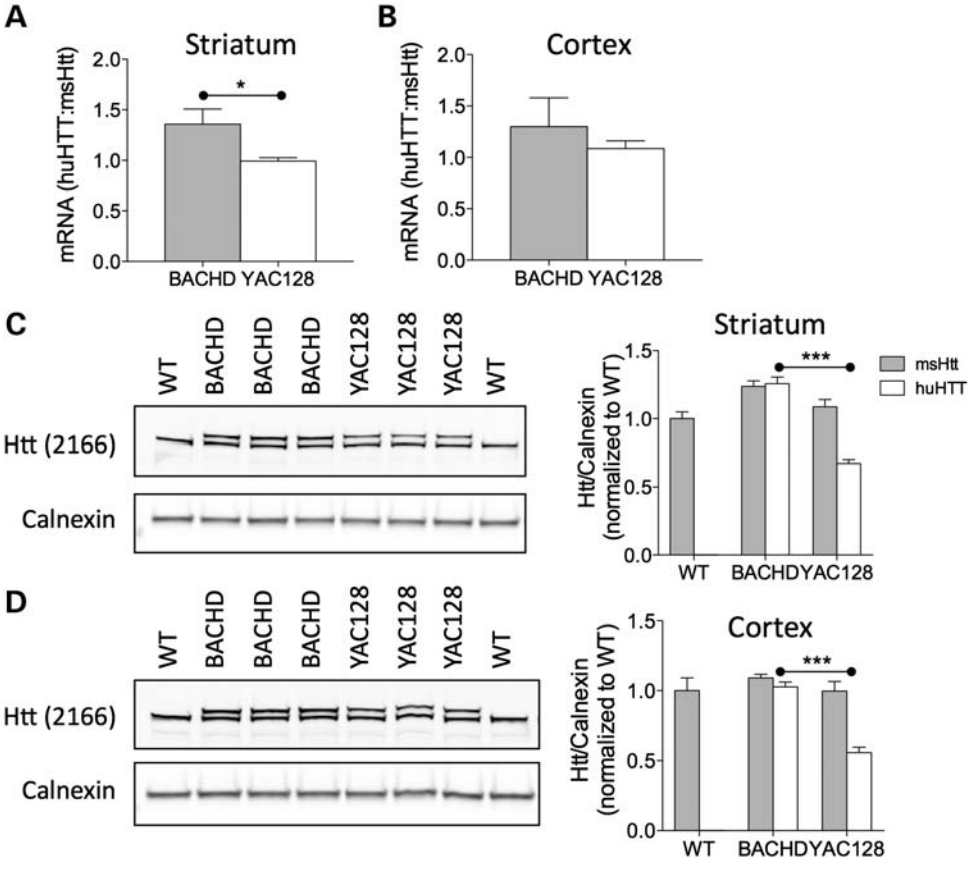

Figure 2. *HTT* and *Hdh* mRNA and protein levels in striatal and cortical tissues from BACHD and YAC128 mice. Levels of *HTT* and *Hdh* mRNA and protein products (huHTT and msHtt) in striatal and cortical tissues of 2-month-old BACHD and YAC128 mice were assessed using quantitative reverse transcription polymerase chain reaction (RT–PCR) (**A** and **B**) and immunoblot (**C** and **D**). mRNA expression levels of *HTT* and *Hdh* genes were normalized to *Actb* (β-actin). The data represent the ratio of *HTT*:*Hdh* mRNA in striatal (A) and cortical (B) tissue of BACHD and YAC128 mice ($n = 4$ for BACHD and 5 for YAC128). HuHTT and msHtt protein levels in striatal (C) and cortical (D) tissues of BACHD and YAC128 mice ($n = 2$ for wild type (WT), 3 for BACHD and 3 for YAC128). All data represent means ± SEM. $^{*}P < 0.05$, and $^{***}P < 0.001$.

human (hu) and mouse (ms) Htt in striatal and cortical tissues of 2-month-old animals. In BACHD mice, striatal levels of huHtt mRNA are ∼1.36× the endogenous msHtt mRNA levels, and are significantly higher in comparison to YAC128 mice where the ratio of huHtt:msHtt mRNA is ∼0.99× (Fig. 2A). Similarly, cortical levels of huHtt mRNA are ∼1.30× those of endogenous msHtt mRNA in BACHD mice compared with 1.09× in the YAC128 mice (Fig. 2B). Consistent with the higher huHtt mRNA levels in BACHD than in YAC128 mice, the levels of the huHtt protein as assessed by monoclonal 2166 anti-htt antibody are significantly higher in BACHD compared with YAC128 mice in both the striatum (Fig. 2C; huHtt:msHtt is ∼1.00× for BACHD and 0.63× for YAC128) and the cortex (Fig. 2D; huHtt:msHtt is ∼0.94× for BACHD and ∼0.56× for YAC128). Similar results are observed with anti-htt BKP1 antibody (data not shown).

Body weight and plasma IGF-1 levels in BACHD and YAC128 mice

We previously reported that the body weight of the mice is influenced by the levels of full-length Htt (23) and this correlated with plasma insulin-like growth factor 1 (IGF-1) levels

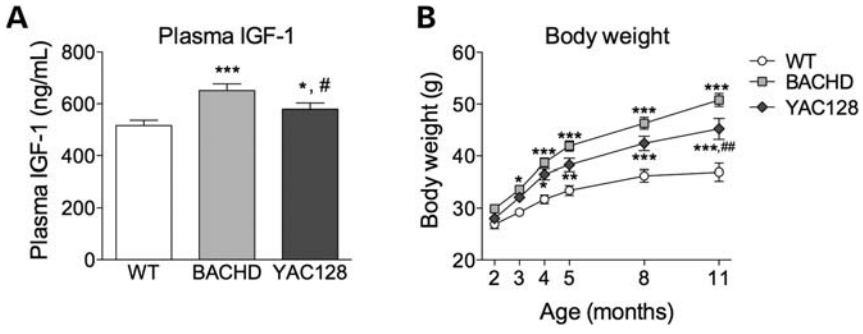

Figure 3. Increased plasma insulin-like growth factor 1 (IGF-1) levels and body weight in BACHD and YAC128 mice. (**A**) Plasma IGF-1 levels were measured in WT, BACHD and YAC128 mice at 2 months of age and were significantly higher in BACHD ($P < 0.001$) and YAC128 ($P < 0.05$) compared with WT mice. Plasma IGF-1 were also significantly higher in BACHD compared with YAC128 mice ($P < 0.05$) ($n = 24$ for WT, 12 for BACHD and 10 for YAC128). (**B**) Body weights of WT, BACHD and YAC128 mice were measured at 2, 3, 4, 5, 8 and 11 months of age. The body weights of BACHD mice were significantly higher than WT animals at 3, 4, 5, 8 and 11 months of age. The body weights of YAC128 were significantly higher than WT mice at 4, 5, 8 and 11 months of age, and significantly lower than BACHD mice at 11 months of age ($n = 19–23$ for WT, 13–15 for BACHD and 14–16 for YAC128). All data represent means ± SEM. $^{*}P < 0.05$, $^{**}P < 0.01$ and $^{***}P < 0.001$ compared with WT; $^{\#}P < 0.05$, and $^{\#\#}P < 0.01$ compared with BACHD.

(24). As the levels of Htt are higher in BACHD than in YAC128 mice, higher levels of plasma IGF-1 and increased body weight in BACHD compared with YAC128 mice might be expected. Measurement of plasma IGF-1 levels showed that they are significantly higher in YAC128 compared with wild type (WT) mice (Fig. 3A). Consistent with the higher level of full-length Htt in BACHD mice, plasma IGF-1 levels were significantly higher in BACHD mice compared with WT and YAC128 mice (Fig. 3A). Body weight measurements followed a pattern similar to that noted for IGF-1 with body weights of YAC128 mice being significantly higher than WT animals, and the body weights of BACHD mice being the highest (Fig. 3B). As such, any phenotypic measures influenced by body weight are likely to be more affected in BACHD than in YAC128 mice.

Cognitive, motor and psychiatric phenotypes in BACHD and YAC128 mice

Next, we employed rotarod training to examine motor learning in WT, BACHD and YAC128 mice at 2 months of age. BACHD mice showed significant deficits in motor learning compared with WT animals as signified by a shorter latency to fall in trials 1, 2 and 3 of the rotarod learning task (Fig. 4A). Similarly, YAC128 mice exhibited a significantly shorter latency to fall in trial 1 of the task compared with WT mice, and were not different compared with BACHD mice (Fig. 4A).

To examine motor function, we evaluated BACHD, YAC128 and WT mice in the accelerating rotarod task at 2, 4, 6, 8, 10 and 12 months of age. BACHD mice showed significantly reduced performance at 4, 6 and 12 months of age compared with WT animals (Fig. 4B). YAC128 mice exhibited a similarly reduced performance on the accelerating rotarod task at 4, 6, 10 and 12 months of age. There was no significant difference in motor function between the YAC128 and BACHD mice (Fig. 4B).

Mice were also subjected to the Porsolt forced swim test (FST) of depression to examine the depressive-like phenotype. Testing of BACHD mice at 12 months of age showed they exhibited increased immobility, signifying a depressive-like phenotype, compared with age-matched WT animals (Fig. 4C). Consistent with our previous observations (25), YAC128 mice showed increased immobility in the FST compared with WT animals, and these changes were not statistically different from those noted in 12-month-old BACHD mice (Fig. 4C).

To examine responses to acoustic startle and sensory-motor gating, BACHD, YAC128 and WT mice were evaluated using the pre-pulse inhibition (PPI) of startle test at 12 months of age. BACHD mice exhibited a reduced startle response compared with WT mice (Fig. 4D). BACHD mice did not exhibit deficits in PPI of startle relative to WT animals at most of the startle intensities tested. However, they showed enhanced PPI of startle relative to WT at 8 dB above background intensity (Fig. 4E). YAC128 mice similarly showed a decreased startle response compared with WT animals (Fig. 4D). YAC128 mice exhibited significant deficits in PPI to startle relative to WT at 16 dB above background intensity, consistent with a previous report (26) (Fig. 4E). Furthermore, the PPI responses of YAC128 mice were significantly lower compared with BACHD mice at pre-pulse intensities of 8 and 16 dB above background (Fig. 4E).

Striatal transcriptional dysregulation was observed in YAC128, but not in BACHD, mice

Transcriptional dysregulation is a well-established feature of HD and deficits in the levels of a number of striatally enriched genes including those coding DARPP-32, Enkephalin (Enk), dopamine receptors D1 and D2 (D1R and D2R, respectively) and cannabinoid receptor 1 (CB1) have been observed in HD brains (27–32). To examine whether these transcriptional changes are also present in the mouse models, striatal tissues from 10-month-old BACHD and YAC128 mice were tested for expression levels of DARPP-32, Enk, D1R, D2R and CB1 using quantitative RT–PCR. Interestingly, striatal expression levels of DARPP-32, Enk, D1R, D2R and CB1 were similar in BACHD and WT mice (Fig. 5A). In contrast, YAC128 mice showed significantly decreased striatal levels of DARPP-32, Enk, D1R, D2R and CB1 compared with WT animals (Fig. 5B), which more closely resembles the changes observed in brain tissue from HD patients.

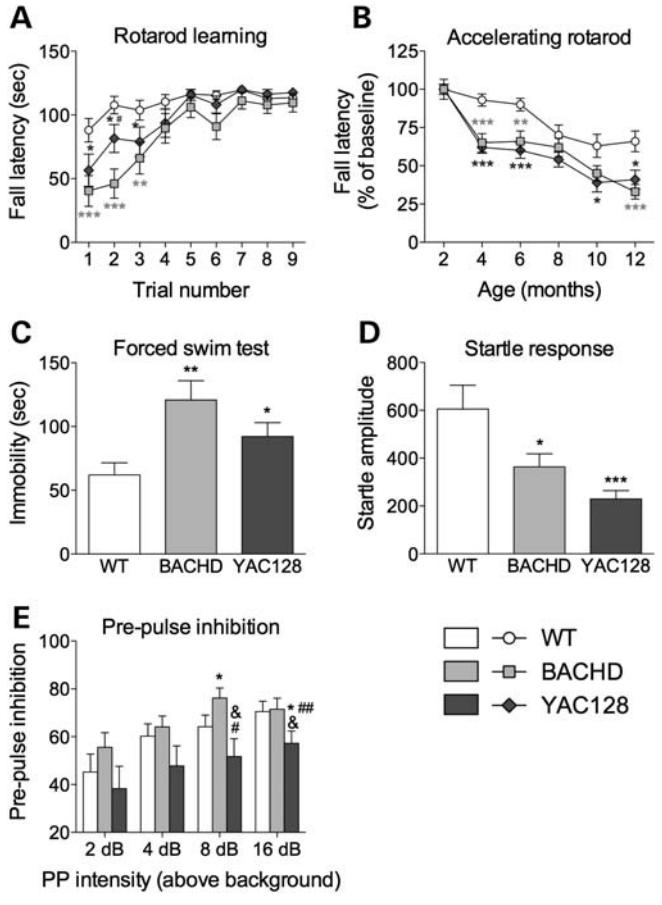

Figure 4. Behavioural abnormalities in BACHD and YAC128 mice. BACHD and YAC128 mice were assessed for motor learning, motor coordination, depressive-like symptoms, startle response and PPI of startle response. (**A**) Motor learning in BACHD and YAC128 mice was assessed using the rotarod task at 2 months of age. Mice were given three 120 s trials per day at a fixed-speed of 18 rpm for three consecutive days, and their latency to fall was recorded. BACHD and YAC128 mice exhibited significant deficits in motor learning compared with WT mice ($^{*}P < 0.05$, $^{**}P < 0.01$, $^{***}P < 0.001$ compared with WT; $^{\#}P < 0.05$ compared with BACHD; $n = 23$ for WT, 15 for YAC128 and 16 for BACHD). (**B**) Motor coordination of BACHD and YAC128 mice was assessed using the accelerating rotarod task at 2, 4, 6, 8, 10 and 12 months of age. BACHD and YAC128 mice exhibited significant deficits in motor coordination compared with WT mice ($^{*}P < 0.05$, $^{**}P < 0.01$, $^{***}P < 0.001$ compared with WT; $n = 16–23$ for WT, 13–16 for BACHD and 13–15 for YAC128). (**C**) The Porsolt FST was used to assess depressive-like symptoms. Both BACHD and YAC128 mice exhibited depressive-like symptoms as signified by increased immobility compared with WT mice ($^{*}P < 0.05$, $^{**}P < 0.01$ compared with WT; $n = 12$ for WT, 6 for BACHD and 9 for YAC128). (**D**) The startle response of BACHD and YAC128 mice to a 120 dB noise burst was measured using an SR-Lab System apparatus. Both BACHD and YAC128 mice exhibited significantly reduced startle response compared with WT mice ($^{*}P < 0.05$, $^{***}P < 0.001$ compared with WT; $n = 19$ for WT, 13 for BACHD and 14 for YAC128). (**E**) The PPI to startle response of BACHD and YAC128 mice was assessed at different startle intensities. The PPI to startle of YAC128 mice was significantly reduced compared with WT at 16 dB above background, and compared with BACHD mice at 8 and 16 dB above background ($^{*}P < 0.05$ compared with WT; $^{\#}P < 0.05$, $^{\#\#}P < 0.01$ compared with BACHD; $^{\&}P < 0.05$ compared with respective response at 2 dB above background; $n = 19$ for WT, 14 for BACHD and 13 for YAC128).

To examine whether the changes in striatal transcripts were paralleled by changes in protein levels, we measured the levels of the DARPP-32 protein in striatal tissues from BACHD and YAC128 mice at 10 months of age. Consistent with the DARPP-32 mRNA levels, we observed no difference in the levels of the striatal DARPP-32 protein between BACHD and WT mice (Fig. 5C), whereas the levels of the striatal DARPP-32 protein were significantly reduced in YAC128 compared with WT mice (Fig. 5D).

Deficits in brain weight and striatal volume in 12-month-old BACHD and YAC128 mice

The forebrain weight, cerebellar weight and striatal volume of the HD mouse models were determined as measures of neuropathology. Both BACHD and YAC128 mice exhibit significantly lower forebrain weight compared with WT animals (Fig. 6A). In contrast, the cerebellar weight of BACHD and YAC128 animals was similar to that of WT animals (Fig. 6B). Also, both BACHD and YAC128 mice showed significantly decreased striatal volume compared with WT animals (Fig. 6C). No difference in forebrain weight, cerebellar weight or striatal volume was observed between BACHD and YAC128 mice (Fig. 6A–C).

Striatal S830-positive aggregates in YAC128, but not in BACHD, mice

Appearance of mHTT aggregates and inclusion bodies is a hallmark of HD neuropathology. Using the S830 antibody previously shown to recognize mHTT aggregates (33,34), immunohistochemistry was performed on striatal sections from 12-month-old BACHD, YAC128 and WT mice. No S830-positive aggregates were detected in striatal sections of BACHD and WT mice (Fig. 7). In contrast, both S830-positive diffuse staining and distinct inclusions were observed throughout the striatum in YAC128 mice (Fig. 7). That no aggregates were detected in the BACHD mice by the S830 antibody does not rule out the possibility that aggregates may be detectable using different antibody or immunohistochemical procedures than the ones employed in this study. The presence of striatal mHTT aggregates in YAC128 HD mice parallels the observations in HD patients.

DISCUSSION

Studies employing the full-length BACHD and YAC128 mouse models of HD have suggested that the nature and natural history of the phenotypic abnormalities in these two models are similar (12,13). Given that the experimental protocols, equipment, housing conditions and background strains employed by different laboratories were varied which may impact the phenotypic features, we sought to determine by direct comparison in the same laboratory the biochemical behavioural and neuropathological characteristics of BACHD and YAC128 HD mouse models on the same background strain using a select set of behavioural tests, biochemical, and neuroanatomical measures. The findings from this comparison showed that although BACHD and YAC128 animals exhibit similar deficits in motor learning and coordination, depressive-like symptoms, striatal volume loss and forebrain weight loss, they differ markedly in key features characteristic

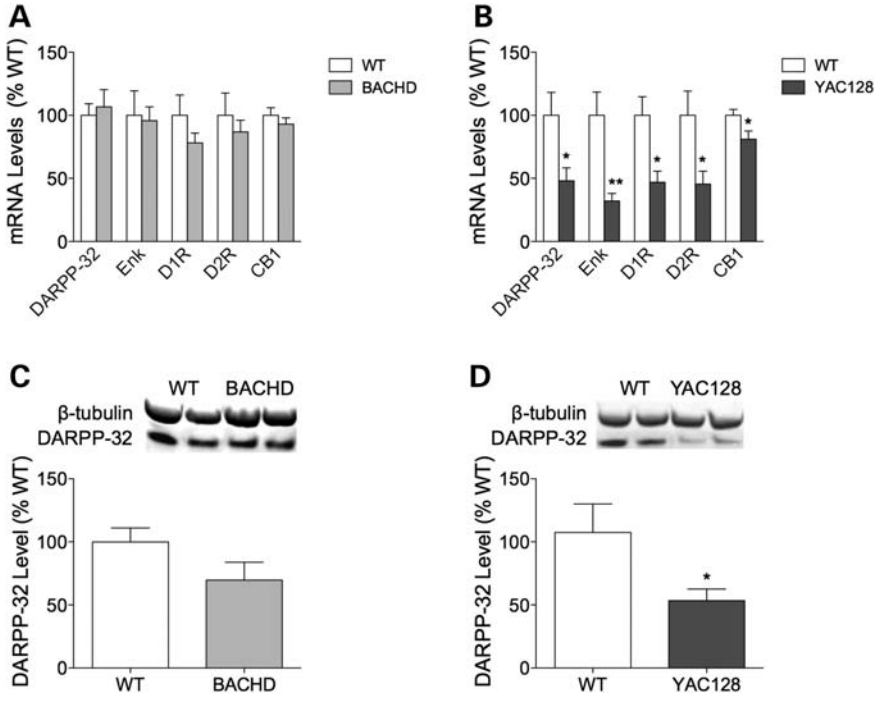

Figure 5. Transcriptional dysregulation in YAC128, but not in BACHD, mice. To examine transcriptional dysregulation in BACHD and YAC128 mice, expression levels of striatal DARPP-32, Enk, D1R, D2R and CB1 were measured using quantitative RT–PCR at 10 months of age. (**A**) Striatal levels of DARPP-32, Enk, D1R, D2R and CB1 mRNA were similar between BACHD and WT mice ($n = 6–7$ for WT, and 6 for BACHD). (**B**) In YAC128 mice, striatal levels of DARPP-32, Enk, D1R, D2R and CB1 mRNA were all significantly decreased compared with WT mice ($n = 8$ for WT, and 6 for YAC128). (**C**) Assessment of protein levels of striatal DARPP-32 by immunoblot analysis revealed no difference between BACHD and WT mice at 10 months of age ($n = 7$ for WT, and 7 for BACHD). (**D**) Striatal protein levels of DARPP-32 were significantly decreased in YAC128 compared with WT mice at 10 months of age ($n = 11$ for WT, and 12 for YAC128). All data represent means ± SEM. $^{*}P < 0.05$, and $^{**}P < 0.01$ compared with WT.

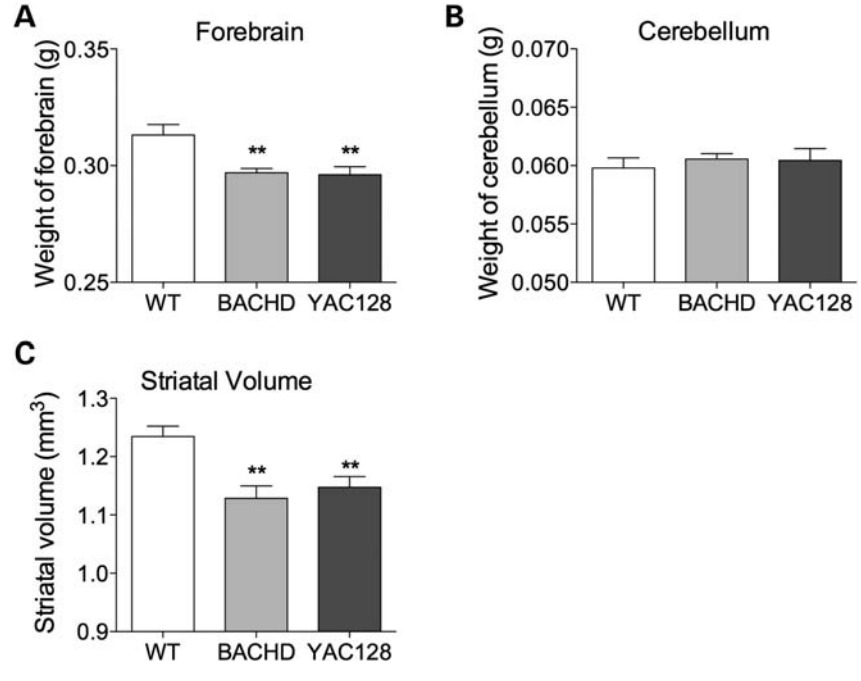

Figure 6. Deficits in brain weight and striatal volume in YAC128 and BACHD mice. Forebrain weight, cerebellar weight and striatal volume were evaluated in 12-month-old mice as measures of neuropathology. (**A**) Both BACHD and YAC128 mice exhibited significant deficits in forebrain weight compared with WT animals ($n = 14$ for WT, 13 for BACHD and 13 for YAC128). (**B**) Cerebellar weight in BACHD and YAC128 mice was similar to that of WT mice ($n = 16$ for WT, 13 for BACHD and 12 for YAC128). (**C**) Both BACHD and YAC128 mice showed significantly decreased striatal volume compared with WT mice ($n = 14$ for WT, 13 for BACHD and 13 for YAC128). All data represent means ± SEM. $^{**}P < 0.01$ compared with WT.

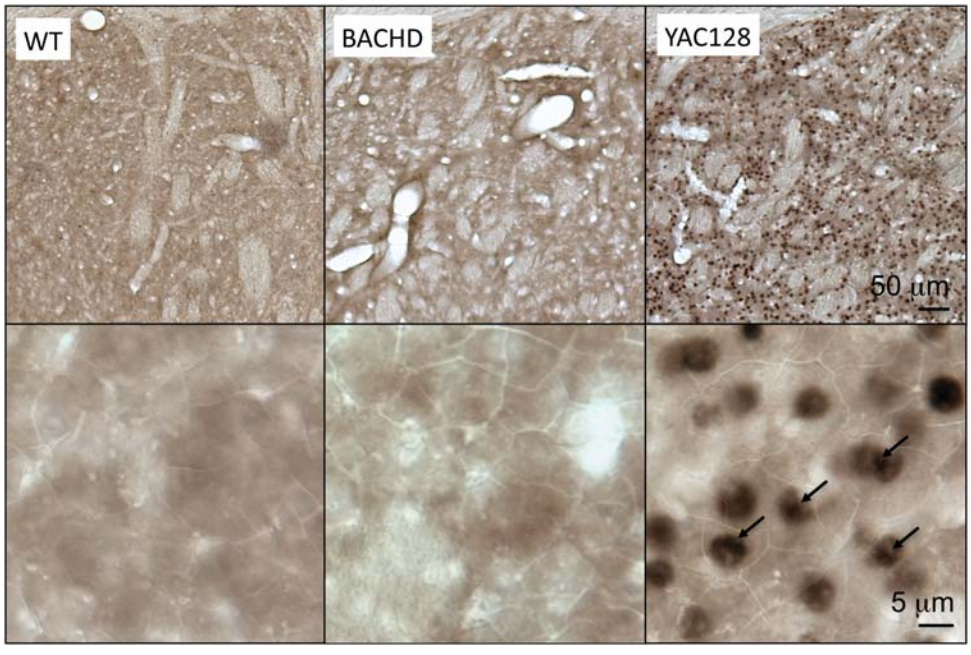

Figure 7. Absence of S830-positive aggregates in striatal tissues of WT and BACHD mice. The presence of striatal mHTT aggregates and inclusion bodies in 12-month-old BACHD and YAC128 mice was examined by immunohistochemistry using the S830 antibody. No S830-positive aggregates were detected in striatal sections of BACHD and WT mice. In contrast, both S830-positive diffuse staining and distinct inclusions were observed throughout the striatum in YAC128 mice.

Table 3. Comparison of characteristic of the BACHD and YAC128 mouse models of HD and human patients

	BACHD mice	YAC128 mice	HD patient
Genetics			
Number of exons	67	67	67
CAG/CAA tract composition	49% CAGs, 49% CAA	Nearly pure CAG tract with penultimate CAA (93% CAG, 7% CAA)	Nearly pure CAG tract with penultimate CAA
Behaviour			
Cognitive function	Deficits in motor learning	Deficits in motor learning and sensory motor gating	Cognitive deficits
Motor coordination	Decreased performance in accelerating rotarod	Decreased performance in accelerating rotarod	Motor deficits
Psychiatric status	Depressive-like phenotype in FST	Depressive-like phenotype in FST	Psychiatric disturbances
Biochemical/metabolic			
Plasma IGF-1 levels	Increased	Increased	?
Body weight	Increased	Increased	Decreased
Transcriptional dysregulation	No change	Decreased levels of DARPP-32, Enk, D1R, D2R, CB1 transcripts	Decreased levels of DARPP-32, Enk, D1R, D2R, CB1 transcripts
Neuropathology			
Forebrain weight	Decreased	Decreased	Decreased
Striatal volume	Decreased	Decreased	Decreased
mHTT aggregates	Not detected	Present	Present

of HD including deficits in the levels of certain striatally enriched transcripts and in the accumulation of S830-positive mHTT aggregates (Table 3).

The body weights of BACHD and YAC128 mice have previously been reported to be higher than those of WT animals (23,24). We now demonstrate that compared with that of YAC128 mice, the body weight of BACHD mice is significantly higher. Levels of full-length Htt and plasma IGF-1 have been shown to influence body weight in transgenic animals, with increased levels of full-length Htt being associated with increased plasma IGF-1 levels and higher body weights (23,24). Our finding that body weight and plasma IGF-1 levels of BACHD mice are significantly higher compared with YAC128 mice is, therefore, consistent with the significantly higher levels of full-length Htt observed in BACHD compared with YAC128 mice. The increased body weight of BACHD mice compared with YAC128 mice is also in agreement with previously published findings (35). These findings also indicate that any potential confounds of the increased body weight observed in these transgenic mice are likely to be of greater impact in the BACHD than in the YAC128 mice.

BACHD and YAC128 animals exhibited similar aberrations in behaviour. Both lines showed deficits in the rotarod test of motor learning compared with WT mice, with a trend towards

worsened performance in the BACHD mice compared with YAC128 animals. BACHD and YAC128 mice also showed similar motor dysfunction in the accelerating rotarod task, an aberrant startle response and depressive-like phenotypes signified by increased immobility in the FST of depression. The increased immobility observed in the BACHD and YAC128 mice is not due to age-dependent motor deficits as we have previously demonstrated that the ability of the mice to swim is not affected by the motor dysfunction they develop [(25); Pouladi *et al*., unpublished data]. Thus, both mouse models are equally useful for studies aiming to investigate and/or modulate these motor and behavioural aspects of the disease.

Although several studies have shown clear deficits in motor coordination in YAC128 mice as assessed by the rotarod task (12,25,36,37), a recent study in which the behavioural phenotypes of BACHD and YAC128 were evaluated demonstrated deficits in rotarod performance in BACHD but not in YAC128 mice (35). This is in contrast to our finding of comparable deficits in rotarod performance in YAC128 and BACHD relative to WT mice. Similarly, the study reported the startle response of BACHD mice to be reduced compared with WT, whereas no deficits in startle response were observed in YAC128 mice (35). These discrepancies may be due to differences in the apparatus, the test procedure or the testing regimens employed. It may also represent an outlier effect as the study reported the rotarod performance of WT mice in the YAC128 cohort to be considerably lower than that of WT mice in the BACHD cohort (35).

BACHD and YAC128 mice also displayed other notable differences. Whereas YAC128 mice exhibited a significant decrease in PPI of startle response compared with WT mice, BACHD mice exhibited a significant increase in PPI of startle response compared with WT mice. PPI of startle response is a measure of sensorimotor gating, the striatally dependent inhibition of involuntary movements. This function is impaired in patients with HD who exhibit decreased PPI of startle response (38). The decrease in YAC128 and increase in BACHD mice of PPI of startle response is consistent with previous reports (26,35), although one study observed no deficits in PPI of startle response in YAC128 mice (35). This discrepancy may be due to differences in the experimental protocol employed.

The altered startle and PPI of startle responses observed in BACHD and YAC128 mice could conceivably reflect hearing impairment. However, this possibility is not supported by the findings which demonstrate while both BACHD and YAC128 mice show decreased startle response compared with WT animals, BACHD mice exhibit increased PPI while YAC128 mice showed decreased PPI compared with WT mice. This disconnect between changes in the startle response and the PPI suggests that the decrease in PPI is unlikely to reflect hearing impairment, and more likely reflects impaired sensorimotor gating in these animals. Additional evidence indicative of functioning hearing abilities in the BACHD and YAC128 mice is the increased PPI observed with increasing pre-pulse intensities. The PPI response in YAC128 mice when subjected to a pre-pulse intensity of 16 dB above background is significantly higher compared with their PPI response when the animals are subjected to a pre-pulse intensity of 2 dB above background. A similar increase in PPI is observed in BACHD mice with increasing pre-pulse intensity (8 dB above background versus 2 dB above background). These findings suggest a functioning yet altered PPI response and sensorimotor gating in BACHD and YAC128 mice.

Furthermore, the performance of YAC128 and BACHD mice in the test of PPI of startle response paralleled the pattern of expression of striatal DARPP-32 in these mice. DARPP-32 has been shown to play a role in mediating PPI of startle response, as animals deficient in DARPP-32 expression exhibit deficits in this test (39). Striatal DARPP-32 levels were reduced in YAC128 but not BACHD mice compared with WT. The deficits in DARPP-32 observed in YAC128 mice are consistent with our previous findings demonstrating decreases in DARPP-32 mRNA and protein levels (36,40–42), and may contribute to the deficits in PPI of startle response in YAC128 mice not seen in BACHD mice. In addition to the deficits in DARPP-32 noted in YAC128 animals, striatal levels of mRNA transcripts encoding Enk, D1R, D2R and CB1 were similarly reduced in 10-month-old YAC128 compared with WT mice. No such deficits in mRNA transcripts of DARPP-32, Enk, D1R, D2R or CB1 were observed in striatal tissue from BACHD compared with WT mice. The lack of change in the mRNA levels of these striatally enriched genes in BACHD mice is in sharp contrast to findings from human HD brains, where, similar to the YAC128 mice, decreases in the levels of DARPP-32, Enk, D1R, D2R and CB1 are observed (27–32). Furthermore, the findings suggest that transcriptional changes do not necessarily represent good surrogate measures for reversal of HD-associated phenotypic deficits, such as motor dysfunction, depressive-like phenotype and neuronal atrophy in all models of HD as indeed these phenotypic deficits are present in BACHD mice despite absence of transcriptional changes in these genes. Moreover, BACHD and YAC128 mice have similar motor performance and striatal atrophy phenotypes, while only YAC128 show transcriptional changes, such as decreases in DARPP-32 levels. This suggests that the mechanism underlying the motor and cognitive dysfunction in BACHD mice is unlikely to relate to decreased DARPP-32. Furthermore, given the similarities in the phenotypic deficits in BACHD and YAC128 mice, it is also possible that the motor and cognitive dysfunction in YAC128 mice is unrelated to the reported transcriptional changes.

Furthermore, similar to findings in brains of HD patients, YAC128 mice displayed widespread striatal aggregates, as assessed by S830-positive staining at 12 months of age, consistent with previous studies demonstrating age-dependent accumulation of mHTT aggregates in striatal and cortical regions of YAC128 mice (12,43). This finding is in sharp contrast to the BACHD mice where no S830-positive aggregates were detected at 12 months of age. Formation of mHTT aggregates has been shown to be influenced by mHTT levels, with increasing levels of mHTT being associated with increasing aggregation and inclusion body formation (44). The lack of S830-positive aggregates in BACHD mice is, therefore, unlikely to be the result of reduced mHTT levels as indeed higher levels of mHTT are observed in BACHD compared with YAC128 mice. These findings support the notion that aggregates detected by this antibody may not represent the toxic species that underlie the pathology of the disease.

Thus, despite the absence of S830-positive mHTT aggregates in BACHD mice, the profile of motor, cognitive and depressive-like deficits and neuropathology was mostly similar to that of YAC128 where widespread S830-positive mHTT aggregates were detected.

However, it should be noted that although no aggregates were detected in the BACHD mice using the S830 antibody, this does not rule out the possibility that aggregates may be detectable using different antibody or immunohistochemical procedures than the ones employed in this study. Indeed, a recent study reports that using the 3B5H10 antibody, mHTT-containing neuropil aggregates were detected in brain sections of BACHD mice following aggressive antigen retrieval involving formic acid (45).

It is not clear what may underlie the differences in the pattern of transcriptional changes and mHTT aggregation between BACHD and YAC128 mice. One possibility may be that these differences are due to differences in the mHTT proteins expressed in the BACHD versus YAC128 mice. Indeed, of 36 SNP alleles that differed between the BACHD and YAC128 *HTT* transgenes, 3 are predicted to result in missense amino acid differences, 1 of which is predicted to affect the physical properties and/or the function of mHTT. It is also conceivable that in addition to these three SNP alleles, other sequence differences influencing the physical properties or the function of the mHTT proteins in the BACHD and YAC128 mice may exist as reflected in differences of 5′ and 3′ lengths. Further studies are needed to investigate the possible impact of these SNP allelic differences on mHTT function and disease phenotype.

An additional factor that may contribute to the phenotypic differences between BACHD and YAC128 mice is the length of the CAG repeat tract in the *HTT* gene. CAG repeat length has been shown to influence the age of disease onset (46–48). As BACHD and YAC128 mice express mutant *HTT* constructs with different CAG repeat lengths (97 for BACHD versus 125 for YAC128 mice), this difference may contribute to their phenotypic differences. However, levels of mutant HTT have also been shown to contribute to rate of progression and disease severity (44,49). In light of the differences in levels of mutant HTT expressed by BACHD and YAC128 mice, the relative contribution of CAG repeat length versus mutant HTT dose to the phenotypic differences between the models may be difficult to determine.

Another factor that may underlie the phenotypic differences between the BACHD and YAC128 mice may relate to the nature of CAG tracts contained in their respective human *HTT* transgenes. Whereas 51% of the CAG tract of the transgene in BACHD mice is composed of CAA trinucleotide repeats (49 CAAs out of 97 CAG/CAA repeats), the CAG tract in YAC128 mice is nearly pure with CAA trinucleotide repeats constituting only ∼7% (9 CAAs out of 125 CAG/CAA repeats). One postulated mechanism by which CAG repeat expansion may lead to neurodegeneration involves RNA transcripts containing expanded CAG tracts forming secondary structures and mediating toxic effects such as misregulation of alternative splicing processes (50,51). The nature of the CAA interruptions in the CAG tract has been shown to heavily influence the secondary structures formed by these expanded CAG tract RNA transcripts, with pure tracts forming slippery hairpins and CAA-interrupted tracts forming branched hairpin structures (52). Thus, the notable differences in the nature of the CAA interruptions of the CAG tracts between BACHD and YAC128 mice may contribute to their differences in the profile of transcriptional dysregulation and the presence of aggregates, possibly by influencing secondary pathways. However, further studies would be needed to investigate this possibility. These findings also suggest that differences in the sequence of the CAG tract and the nature of the CAA interruptions do not represent major contributors to the behavioural deficits and striatal atrophy observed in the BACHD and YAC128 HD mice.

In summary, our study demonstrates that while BACHD and YAC128 animals exhibit similar deficits in motor learning and coordination, depressive-like symptoms and striatal atrophy, they show differences in key features characteristic of HD, including the profile of transcriptional dysregulation as well as the presence of S830-positive mHTT aggregates. These findings illuminate key differences between the models that may serve to guide the selection of distinct useable endpoints in trials of therapeutic agents in the YAC128 and BACHD mice.

MATERIALS AND METHODS

Animals

Male and female YAC128 and BACHD mice expressing expanded human huntingtin with 125 and 97 CAG repeats, respectively, and WT littermates maintained on the FVB/N strain (Charles River, Wilmington, MA, USA) were used (12,13). Mice were housed with littermates of mixed genotype. Animals were maintained under a 12 h L:12 h D light cycle (lights on at 2300) in a clean facility and given free access to food and water. Experimenters were blind to the genotype of the mice. Experiments were performed with the approval of the animal care committee at the University of British Columbia.

Rotarod test of motor learning and motor coordination

Training and baseline testing for motor function tasks was carried at 2 months of age. Testing took place during the dark cycle and was carried out every 2 months between 2 and 12 months of age. Motor learning, and motor coordination and balance were assessed using accelerating rotarod tasks (UGO Basile, Comerio, Italy). For training, mice were given three 120 s trials per day at a fixed-speed of 18 rpm for three consecutive days. During the testing phase, the rotarod accelerated from 5 to 40 rpm over 5 min; the maximum score was 300 s. Rotarod scores are the average of three trials spaced 2 h apart.

Porsolt FST of depression

The Porsolt FST was performed as described previously (25). Briefly, mice were placed in individual cylinders (25 cm tall × 19 cm wide) filled with room temperature water (23–25°C) to a depth of 15 cm for a period of 6 min. The test sessions were recorded by a video camera placed directly above the cylinders. The sessions were examined blind and the last 4 min

of the test session was scored using a time-sampling technique to rate the predominant behaviour over 5 s intervals. The following behaviours were measured and recorded at the end of every 5 s: swimming/climbing and immobility. Increased immobility is interpreted as measure of depressive state (53).

Test of PPI

The PPI test of sensorimotor gating was performed using four SR-Lab Systems (San Diego Instruments) as described previously (26). Before testing, the sensitivity of the startle chambers was calibrated using a vibrating standardization unit at 700 V (San Diego Instruments). Mice were then placed into each startle chamber and given a 5 min acclimatization period with background noise alone (65 dB). Each mouse was presented with six trials (block 1) of a 40 ms, 120 dB noise burst (pulse alone). Subsequently, the mice experienced eight blocks of 6 trials (48 trials total), each block consisting of the following trial types: (1) no stimulus (background noise only); (2) a 40 ms, 120 dB noise burst alone; or (3–6) a 40 ms, 120 dB noise burst preceded 100 ms by a 20 ms prepulse (2, 4, 8 and 16 dB above background noise). The order of trials within each block of six trials was pseudo-randomized, and four of the eight blocks contained one extra pulse-alone trial. The mice then received another six trials (block 10) of 40 ms, 120 dB noise burst (pulse alone).The inter-trial interval was randomized throughout the entire session and ranged between 8 and 23 s. Each animal enclosure was wiped clean with ethanol between test subjects. PPI was calculated from the average of six trials per pre-pulse as follows: PPI = [(pulse-alone startle)-(prepulse + pulse startle)]/pulse-alone startle.

Real-time quantitative RT–PCR

HTT and Hdh measurements. Total RNA was extracted from the mouse cortex or striatum with RNeasy Mini Kit or RNeasy Micro Kit (Qiagen) and treated with Amplification Grade DNaesI (Invitrogen). First-strand cDNA was prepared from 1 μg (cortex) or 180 ng (striatum) of total RNA using SuperScriptIII First-Strand Synthesis System (Invitrogen). cDNA generated from 2 ng of input RNA was used in a final volume of 10 μl with Power SYBR Green PCR Master Mix (ABI). Comparative Ct assay was performed using ABI 7500 Fast Real-Time PCR System under default condition. The relative amount of mRNA in each well was calculated as the ratio between the target mRNA and a normalization factor calculated from the endogenous levels of the *Actb* (β-actin) reference gene. *HTT* and mouse *Actb* primers were as described (44). *Hdh* primers were: 5′ TGCTACACCTGAC AGCGAGTCT 3′ and 5′ ATCCCTTGCGGATCCTATCA 3′.

DARPP-32, enkephalin, D1R, D2R and CB1 measurements. Brain tissue samples from S2 were used. Total RNA was extracted using Ambion MagMAX-96 RNA isolation kit (Applied Biosystems). The RNA was reverse-transcribed and amplified using TaqMan® One-Step RT–PCR Master Mix Kit (Applied Biosystems) according to the manufacture's instructions. Quantitative RT–PCR reactions were conducted and analysed on an ABI PRISM® 7500 Real Time PCR System (Applied Biosystems). Expression levels for mRNA were normalized to hypoxanthine guanine phosphoribosyl transferase 1 (*Hprt1*) mRNA levels. Standard curves were created using 10-fold serial dilutions mouse brain cDNA. Each sample was run in duplicate. The relative amount of mRNA in each well was calculated as the ratio between the target mRNA and a normalization factor calculated from the endogenous levels of the *Hprt1* reference gene. The following primer probe sets (Applied Biosystems) were used: DARPP-32 (*Ppp1r1b*), Mm00454892_m1; mouse *Hprt*, Mm00446968_m1; Dopamine Receptor 1(D1; *Drd1a*), Mm01353211_m1; Dopamine Receptor 2 (D2; *Drd2*), Mm00438545_m1; Cannabanoid Receptor 1 (CB1), Mm00432621_s1; Enkephalin (enk; *Penk*), Mm01212875_m1.

Immunoblotting and protein analysis

Htt protein immunoblots. The mouse cortex or striatum protein lysates were prepared as previously described (12). Protein concentration was determined by BioRad Bradford Assay and 25 μg was run on 3–8% NuPAGE Tris-Acetate gels (Invitrogen) and transferred to Immobilon-PVDF-FL membranes. Immunoblots for huntingtin were conducted using mAb2166 (Chemicon, Temecula, CA, USA) and Calnexin (Sigma) antibodies. Calnexin was used as loading control.

DARPP-32 protein immunoblots. Tissues were homogenized in T-PER lysis buffer (Pierce, Rockford, IL, USA) containing a cocktail of protease inhibitors (Complete®; Roche, Germany). After centrifugation, lysates (20 μg/lane) were resolved on a 4–12% SDS–PAGE and transferred to nitrocellulose membrane. Membranes were probed with rabbit anti-DARPP-32 (1:100) polyclonal antibody (Cell Signaling Technology, Beverly, MA, USA) and an anti-β-tubulin (1:1000) polyclonal antibody (Santa Cruz Biotechnology, Santa Cruz, CA, USA). β-Tubulin was used as a loading control.

All immunoblots followed standard procedures and used infrared-labelled secondary antibodies. Protein bands were visualized and quantified using Odyssey software (LI-COR Biosciences).

CAG tract sequencing

A 1.3 kb fragment of *HTT* containing the CAG tract was amplified using human-specific primers from genomic DNA extracted from YAC128 or BACHD mouse tail clip. The amplicon was purified using Qiaquick PCR Purification Kit (Qiagen) and submitted for sequencing. The sequence analysis was performed by ABI Prism 3130xl Genetic Analyzer (Applied Biosystem) using the following primers: 5′-ATT ACAGTCTCACCACGCCC-3′ and 5′-GACAAGGGAAGAC CCAAGTG-3′.

Plasma IGF-1 measurements

To obtain plasma, 2-month-old mice were bled from the saphenous vein with ethylenediaminetetraacetic acid-coated capillary tubes (Sarstedt, Germany). Blood was centrifuged for 10 min at 3500 rpm and plasma was transferred to an

eppendorf tube and stored at −80 C until analysis. Plasma IGF-1 levels were measured using Quantikine Mouse IGF-1 ELISA assay (R&D Systems) as per the manufacturer's instructions.

Brain sample preparation

Mice were injected with heparin followed by terminal anaesthesia with intraperitoneally injected 2.5% avertin. The animals were perfused with phosphate-buffered saline (PBS) followed by ice-cold 4% paraformaldehyde in PBS. Brains were removed and left in 4% paraformaldehyde for 24 h, and then stored in PBS. After weighing, the brains were transferred to a 30% sucrose solution containing 0.08% sodium azide in PBS. They were then frozen on dry ice, mounted with Tissue-TEK O.C.T. compound (Sakura, Torrance, CA, USA) and sliced coronally into 25 μm sections on a cryostat (Microm HM 500M, Richard-Allan Scientific, Kalamazoo, MI, USA). The sections are collected and stored in PBS with 0.08% sodium azide at 4°.

Immunohistochemistry and stereological measurements

A series of 25 μm thick coronal sections spaced 200 μm apart spanning the striatum were stained with NeuN antibody (1:100; Chemicon) overnight at room temperature, followed by incubation with biotinylated anti-mouse antibody (1:200; Vector Laboratories, Burlingame, CA, USA). The signal was amplified with an ABC Elite kit (Vector) and detected with diaminobenzidine (Pierce). Striatal volumes were determined from a series of mounted sections using StereoInvestigator software (Microbrightfield, Williston, VT, USA) by tracing the perimeter of the striatum in serial sections spanning the striatum. For S830 staining, tissue was treated with 10% methanol/1% H_2O_2 for 10 min followed by 3 × 5 min PBS washes. Tissue was blocked in Tris–buffered saline (TBS; 50 mM Tris–HCl, 0.15 M NaCl, pH 7.6, 0.15 M NaCl)/0.1% Triton X-100/5% donkey serum (TBS-TDS) for 1.5 h. After a wash in PBS, sections were incubated with sheep polyclonal S830 antibody (1:2000; generous gift from Dr G. Bates, UK) in TBS-TDS at 4° overnight. Sections incubated without primary antibody served as controls. Following a wash in PBS, sections were incubated with biotinylated donkey anti-sheep secondary antibody (1:500, Jackson ImmunoResearch Labs, West Grove, PA, USA) for 2 h in TBS-TDS. Following a wash in PBS, sections were incubated in Vectastain Elite ABC reagent (Vector Labs Inc., Burlingame, CA, USA) for 0.5 h. Staining was visualized using 3,3′-diaminobenzidine in 50 mM Tris-imidazole buffer (pH 7.6). After being mounted on slides, sections were dehydrated through a graded series of ethanol solutions (70, 85, 90, 100% for 2 min each). Slides were then treated with Citrisolv (Fisher, Tustin, CA, USA) for 2 min, followed by xylene for 10 min and cover slipped with Cytoseal 60 (Richard-Allan Scientific). Sections were photographed using a Zeiss Axioplan 2 microscope and Coolsnap HQ Digital CCD camera (Photometrics, Tucson, AZ, USA). Digital images were colour balanced using Adobe Photoshop 7.0 (Adobe Systems, San Jose, CA, USA).

Statistical analysis

Data are expressed as means ± SEM. Pair-wise comparisons between genotypes/treatments at individual time points were assessed with a Student's *t*-test. Differences were considered statistically significant when $P < 0.05$.

Conflict of Interest statement. None declared.

FUNDING

We thank Dr Gillian Bates for providing the S830 antibody. M.A.P. is the recipient of the BC Innovation Council Ripples of Hope Award in Biotechnology & Entrepreneurship and doctoral awards from the Canadian Institute of Health Research and the Michael Smith Foundation for Health Research. M.R.H. is supported by grants from the Canadian Institutes of Health Research, the Huntington Society of Canada, the Huntington's Disease Society of America, and the CHDI Foundation. M.R.H. is a Killam University Professor and holds a Canada Research Chair in Human Genetics.

REFERENCES

1. The Huntington's Disease Collaborative Research Group. (1993) A novel gene containing a trinucleotide repeat that is expanded and unstable on Huntington's disease chromosomes. *Cell*, **72**, 971–983.
2. Hodgson, J.G., Smith, D.J., McCutcheon, K., Koide, H.B., Nishiyama, K., Dinulos, M.B., Stevens, M.E., Bissada, N., Nasir, J., Kanazawa, I. *et al.* (1996) Human huntingtin derived from YAC transgenes compensates for loss of murine huntingtin by rescue of the embryonic lethal phenotype. *Hum. Mol. Genet.*, **5**, 1875–1885.
3. Menalled, L.B., Sison, J.D., Wu, Y., Olivieri, M., Li, X.-J., Li, H., Zeitlin, S. and Chesselet, M.-F. (2002) Early motor dysfunction and striosomal distribution of huntingtin microaggregates in Huntington's disease knock-in mice. *J. Neurosci.*, **22**, 8266–8276.
4. Yu, Z.-X., Li, S.-H., Evans, J., Pillarisetti, A., Li, H. and Li, X.-J. (2003) Mutant huntingtin causes context-dependent neurodegeneration in mice with Huntington's disease. *J. Neurosci.*, **23**, 2193–2202.
5. Luthi-Carter, R., Strand, A., Peters, N.L., Solano, S.M., Hollingsworth, Z.R., Menon, A.S., Frey, A.S., Spektor, B.S., Penney, E.B., Schilling, G. *et al.* (2000) Decreased expression of striatal signaling genes in a mouse model of Huntington's disease. *Hum. Mol. Genet.*, **9**, 1259–1271.
6. Schilling, G., Coonfield, M.L., Ross, C.A. and Borchelt, D.R. (2001) Coenzyme Q10 and remacemide hydrochloride ameliorate motor deficits in a Huntington's disease transgenic mouse model. *Neurosci. Lett.*, **315**, 149–153.
7. Ferrante, R.J., Andreassen, O.A., Dedeoglu, A., Ferrante, K.L., Jenkins, B.G., Hersch, S.M. and Beal, M.F. (2002) Therapeutic effects of coenzyme Q10 and remacemide in transgenic mouse models of Huntington's disease. *J. Neurosci.*, **22**, 1592–1599.
8. Huntington Study Group. (2001) A randomized, placebo-controlled trial of coenzyme Q10 and remacemide in Huntington's disease. *Neurology*, **57**, 397–404.
9. Schiefer, J., Landwehrmeyer, G.B., Luesse, H.G., Sprunken, A., Puls, C., Milkereit, A., Milkereit, E. and Kosinski, C.M. (2002) Riluzole prolongs survival time and alters nuclear inclusion formation in a transgenic mouse model of Huntington's disease. *Mov. Disord.*, **17**, 748–757.
10. Landwehrmeyer, G.B., Dubois, B., de Yebenes, J.G., Kremer, B., Gaus, W., Kraus, P.H., Przuntek, H., Dib, M., Doble, A., Fischer, W. *et al.* (2007) Riluzole in Huntington's disease: a 3-year, randomized controlled study. *Ann. Neurol.*, **62**, 262–272.
11. Hodgson, J.G., Agopyan, N., Gutekunst, C.A., Leavitt, B.R., LePiane, F., Singaraja, R., Smith, D.J., Bissada, N., McCutcheon, K., Nasir, J. *et al.* (1999) A YAC mouse model for Huntington's disease with full-length mutant huntingtin, cytoplasmic toxicity, and selective striatal neurodegeneration. *Neuron*, **23**, 181–192.

12. Slow, E.J., van Raamsdonk, J., Rogers, D., Coleman, S.H., Graham, R.K., Deng, Y., Oh, R., Bissada, N., Hossain, S.M., Yang, Y.-Z. *et al.* (2003) Selective striatal neuronal loss in a YAC128 mouse model of Huntington disease. *Hum. Mol. Genet.*, **12**, 1555–1567.
13. Gray, M., Shirasaki, D.I., Cepeda, C., André, V.M., Wilburn, B., Lu, X.-H., Tao, J., Yamazaki, I., Li, S.-H., Sun, Y.E. *et al.* (2008) Full-length human mutant huntingtin with a stable polyglutamine repeat can elicit progressive and selective neuropathogenesis in BACHD mice. *J. Neurosci.*, **28**, 6182–6195.
14. Carroll, J.B., Warby, S.C., Southwell, A.L., Doty, C.N., Greenlee, S., Skotte, N., Hung, G., Bennett, C.F., Freier, S.M. and Hayden, M.R. (2011) Potent and selective antisense oligonucleotides targeting single-nucleotide polymorphisms in the huntington disease gene / allele-specific silencing of mutant Huntingtin. *Mol. Ther.*, **19**, 2178–2185.
15. Adzhubei, I.A., Schmidt, S., Peshkin, L., Ramensky, V.E., Gerasimova, A., Bork, P., Kondrashov, A.S. and Sunyaev, S.R. (2010) A method and server for predicting damaging missense mutations. *Nat. Meth.*, **7**, 248–249.
16. Consortium, I.H., Frazer, K.A., Ballinger, D.G., Cox, D.R., Hinds, D.A., Stuve, L.L., Gibbs, R.A., Belmont, J.W., Boudreau, A., Hardenbol, P. *et al.* (2007) A second generation human haplotype map of over 3.1 million SNPs. *Nature*, **449**, 851–861.
17. Sherry, S.T., Ward, M.H., Kholodov, M., Baker, J., Phan, L., Smigielski, E.M. and Sirotkin, K. (2001) dbSNP: the NCBI database of genetic variation. *Nucleic Acids Res.*, **29**, 308–311.
18. Ehrnhoefer, D.E., Sutton, L. and Hayden, M.R. (2011) Small changes, big impact: posttranslational modifications and function of huntingtin in Huntington disease. *Neuroscientist*, **17**, 475–492.
19. Robertson, G., Bilenky, M., Lin, K., He, A., Yuen, W., Dagpinar, M., Varhol, R., Teague, K., Griffith, O.L., Zhang, X. *et al.* (2006) cisRED: a database system for genome-scale computational discovery of regulatory elements. *Nucleic Acids Res.*, **34**, D68–D73.
20. Andersen, M.C., Engström, P.G., Lithwick, S., Arenillas, D., Eriksson, P., Lenhard, B., Wasserman, W.W. and Odeberg, J. (2008) In silico detection of sequence variations modifying transcriptional regulation. *PLoS Comput. Biol.*, **4**, e5.
21. Friedman, R.C., Farh, K.K.-H., Burge, C.B. and Bartel, D.P. (2009) Most mammalian mRNAs are conserved targets of microRNAs. *Genome Res.*, **19**, 92–105.
22. Goldberg, Y.P., McMurray, C.T., Zeisler, J., Almqvist, E., Sillence, D., Richards, F., Gacy, A.M., Buchanan, J., Telenius, H. and Hayden, M.R. (1995) Increased instability of intermediate alleles in families with sporadic Huntington disease compared to similar sized intermediate alleles in the general population. *Hum. Mol. Genet.*, **4**, 1911–1918.
23. Van Raamsdonk, J.M., Gibson, W.T., Pearson, J., Murphy, Z., Lu, G., Leavitt, B.R. and Hayden, M.R. (2006) Body weight is modulated by levels of full-length huntingtin. *Hum. Mol. Genet.*, **15**, 1513–1523.
24. Pouladi, M.A., Xie, Y., Skotte, N.H., Ehrnhoefer, D.E., Graham, R.K., Kim, J.E., Bissada, N., Yang, X.W., Paganetti, P., Friedlander, R.M. *et al.* (2010) Full-length huntingtin levels modulate body weight by influencing insulin-like growth factor 1 expression. *Hum. Mol. Genet.*, **19**, 1528–1538.
25. Pouladi, M.A., Graham, R.K., Karasinska, J.M., Xie, Y., Santos, R.D., Petersén, A. and Hayden, M.R. (2009) Prevention of depressive behaviour in the YAC128 mouse model of Huntington disease by mutation at residue 586 of huntingtin. *Brain*, **132**, 919–932.
26. Van Raamsdonk, J.M., Pearson, J., Slow, E.J., Hossain, S.M., Leavitt, B.R. and Hayden, M.R. (2005) Cognitive dysfunction precedes neuropathology and motor abnormalities in the YAC128 mouse model of Huntington's disease. *J. Neurosci.*, **25**, 4169–4180.
27. Richfield, E.K., Maguire-Zeiss, K.A., Cox, C., Gilmore, J. and Voorn, P. (1995) Reduced expression of preproenkephalin in striatal neurons from Huntington's disease patients. *Ann. Neurol.*, **37**, 335–343.
28. Augood, S.J., Faull, R.L. and Emson, P.C. (1997) Dopamine D1 and D2 receptor gene expression in the striatum in Huntington's disease. *Ann. Neurol.*, **42**, 215–221.
29. Augood, S.J., Faull, R.L., Love, D.R. and Emson, P.C. (1996) Reduction in enkephalin and substance P messenger RNA in the striatum of early grade Huntington's disease: a detailed cellular *in situ* hybridization study. *Neuroscience*, **72**, 1023–1036.
30. Desplats, P.A., Kass, K.E., Gilmartin, T., Stanwood, G.D., Woodward, E.L., Head, S.R., Sutcliffe, J.G. and Thomas, E.A. (2006) Selective deficits in the expression of striatal-enriched mRNAs in Huntington's disease. *J. Neurochem.*, **96**, 743–757.
31. Sugars, K.L. and Rubinsztein, D.C. (2003) Transcriptional abnormalities in Huntington disease. *Trends Genet.*, **19**, 233–238.
32. Okazawa, H. (2003) Polyglutamine diseases: a transcription disorder? Cell. *Mol. Life Sci.*, **60**, 1427–1439.
33. Sathasivam, K., Woodman, B., Mahal, A., Bertaux, F., Wanker, E.E., Shima, D.T. and Bates, G.P. (2001) Centrosome disorganization in fibroblast cultures derived from R6/2 Huntington's disease (HD) transgenic mice and HD patients. *Hum. Mol. Genet.*, **10**, 2425–2435.
34. Hockly, E., Richon, V.M., Woodman, B., Smith, D.L., Zhou, X., Rosa, E., Sathasivam, K., Ghazi-Noori, S., Mahal, A., Lowden, P.A.S. *et al.* (2003) Suberoylanilide hydroxamic acid, a histone deacetylase inhibitor, ameliorates motor deficits in a mouse model of Huntington's disease. *Proc. Natl Acad. Sci. USA*, **100**, 2041–2046.
35. Menalled, L., El-Khodor, B.F., Patry, M., Suárez-Fariñas, M., Orenstein, S.J., Zahasky, B., Leahy, C., Wheeler, V., Yang, X.W., MacDonald, M. *et al.* (2009) Systematic behavioral evaluation of Huntington's disease transgenic and knock-in mouse models. *Neurobiol. Dis.*, **35**, 319–336.
36. Van Raamsdonk, J.M., Pearson, J., Bailey, C.D.C., Rogers, D.A., Johnson, G.V.W., Hayden, M.R. and Leavitt, B.R. (2005) Cystamine treatment is neuroprotective in the YAC128 mouse model of Huntington disease. *J. Neurochem.*, **95**, 210–220.
37. Graham, R.K., Deng, Y., Slow, E.J., Haigh, B., Bissada, N., Lu, G., Pearson, J., Shehadeh, J., Bertram, L., Murphy, Z. *et al.* (2006) Cleavage at the caspase-6 site is required for neuronal dysfunction and degeneration due to mutant huntingtin. *Cell*, **125**, 1179–1191.
38. Swerdlow, N.R., Paulsen, J., Braff, D.L., Butters, N., Geyer, M.A. and Swenson, M.R. (1995) Impaired prepulse inhibition of acoustic and tactile startle response in patients with Huntington's disease. *J. Neurol. Neurosur. Psychiatry*, **58**, 192–200.
39. Svenningsson, P., Tzavara, E.T., Carruthers, R., Rachleff, I., Wattler, S., Nehls, M., McKinzie, D.L., Fienberg, A.A., Nomikos, G.G. and Greengard, P. (2003) Diverse psychotomimetics act through a common signaling pathway. *Science*, **302**, 1412–1415.
40. Metzler, M., Gan, L., Mazarei, G., Graham, R.K., Liu, L., Bissada, N., Lu, G., Leavitt, B.R. and Hayden, M.R. (2010) Phosphorylation of huntingtin at Ser421 in YAC128 neurons is associated with protection of YAC128 neurons from NMDA-mediated excitotoxicity and is modulated by PP1 and PP2A. *J. Neurosci.*, **30**, 14318–14329.
41. Van Raamsdonk, J.M., Pearson, J., Rogers, D.A., Bissada, N., Vogl, A.W., Hayden, M.R. and Leavitt, B.R. (2005) Loss of wild-type huntingtin influences motor dysfunction and survival in the YAC128 mouse model of Huntington disease. *Hum. Mol. Genet.*, **14**, 1379–1392.
42. Van Raamsdonk, J.M., Pearson, J., Rogers, D.A., Lu, G., Barakauskas, V.E., Barr, A.M., Honer, W.G., Hayden, M.R. and Leavitt, B.R. (2005) Ethyl-EPA treatment improves motor dysfunction, but not neurodegeneration in the YAC128 mouse model of Huntington disease. *Exp. Neurol.*, **196**, 266–272.
43. Van Raamsdonk, J.M., Murphy, Z., Slow, E.J., Leavitt, B.R. and Hayden, M.R. (2005) Selective degeneration and nuclear localization of mutant huntingtin in the YAC128 mouse model of Huntington disease. *Hum. Mol. Genet.*, **14**, 3823–3835.
44. Graham, R.K., Slow, E.J., Deng, Y., Bissada, N., Lu, G., Pearson, J., Shehadeh, J., Leavitt, B.R., Raymond, L.A. and Hayden, M.R. (2006) Levels of mutant huntingtin influence the phenotypic severity of Huntington disease in YAC128 mouse models. *Neurobiol. Dis.*, **21**, 444–455.
45. Miller, J., Arrasate, M., Brooks, E., Libeu, C.P., Legleiter, J., Hatters, D., Curtis, J., Cheung, K., Krishnan, P., Mitra, S. *et al.* (2011) Identifying polyglutamine protein species *in situ* that best predict neurodegeneration. *Nat. Chem. Biol.*, **7**, 925–934.
46. Andrew, S.E., Goldberg, Y.P., Kremer, B., Telenius, H., Theilmann, J., Adam, S., Starr, E., Squitieri, F., Lin, B., Kalchman, M.A. *et al.* (1993) The relationship between trinucleotide (CAG) repeat length and clinical features of Huntington's disease. *Nat. Genet.*, **4**, 398–403.
47. Brinkman, R.R., Mezei, M.M., Theilmann, J., Almqvist, E. and Hayden, M.R. (1997) The likelihood of being affected with Huntington disease by a particular age, for a specific CAG size. *Am. J. Hum. Genet.*, **60**, 1202–1210.
48. Langbehn, D.R., Brinkman, R.R., Falush, D., Paulsen, J.S. and Hayden, M.R. (2004) A new model for prediction of the age of onset and

penetrance for Huntington's disease based on CAG length. *Clin. Genet.*, **65**, 267–277.
49. Squitieri, F., Gellera, C., Cannella, M., Mariotti, C., Cislaghi, G., Rubinsztein, D.C., Almqvist, E.W., Turner, D., Bachoud-Levi, A.C., Simpson, S.A. *et al.* (2003) Homozygosity for CAG mutation in Huntington disease is associated with a more severe clinical course. *Brain*, **126**, 946–955.
50. Sobczak, K., de Mezer, M., Michlewski, G., Krol, J. and Krzyzosiak, W.J. (2003) RNA structure of trinucleotide repeats associated with human neurological diseases. *Nucleic Acids Res.*, **31**, 5469–5482.
51. Mykowska, A., Sobczak, K., Wojciechowska, M., Kozlowski, P. and Krzyzosiak, W.J. (2011) CAG repeats mimic CUG repeats in the misregulation of alternative splicing. *Nucleic Acids Res.*, **39**, 8938–8951.
52. Sobczak, K. and Krzyzosiak, W.J. (2005) CAG repeats containing CAA interruptions form branched hairpin structures in spinocerebellar ataxia type 2 transcripts. *J. Biol. Chem.*, **280**, 3898–3910.
53. Cryan, J.F., Markou, A. and Lucki, I. (2002) Assessing antidepressant activity in rodents: recent developments and future needs. *Trends Pharmacol. Sci.*, **23**, 238–245.